

**ANALYSIS AND COMPARISON OF AIRFOIL-POLAR  
PREDICTION METHODS FOR VERTICAL-AXIS  
TURBINES**

**GOH SU TENG**

**SCHOOL OF AEROSPACE ENGINEERING  
UNIVERSITI SAINS MALAYSIA**

**2021**

# **ANALYSIS AND COMPARISON OF AIRFOIL-POLAR PREDICTION METHODS FOR VERTICAL-AXIS TURBINES**

**by**

**GOH SU TENG**

**Thesis submitted in fulfilment of the requirements for the  
Bachelor Degree of Engineering (Honours) (Aerospace Engineering)**

**June 2021**

## ENDORSEMENT

I, Goh Su Teng hereby declare that I have checked and revised the whole draft of dissertation as required by my supervisor.



---

(Signature of Student)

Date: 9 July 2021



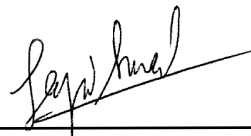
---

(Signature of Supervisor)

Name:

Assoc. Prof. Dr. Ahmad Zulfaa Mohamed Kassim

Date: 9 July 2021



---

(Signature of Examiner)

Name:

Assoc. Prof. Dr. Farzad Ismail

Date: 10 July 2021

## DECLARATION

This thesis is the result of my own investigation, except where otherwise stated and has not previously been accepted in substance for any degree and is not being concurrently submitted in candidature for any other degree.

A handwritten signature in black ink, appearing to be 'A. S. R.', written above a horizontal line.

(Signature of Student)

Date: 9 July 2021

## **ACKNOWLEDGEMENT**

This final year project is for the completion of degree of Bachelor of Aerospace Engineering. Support and commitments from several individuals have contributed to the success in completion of my final year project. Therefore, I would like to show my highest gratitude and appreciation to all the individuals involved for their contribution throughout the project.

First and foremost, I would like to express my sincere appreciation to my supervisor, Assoc. Prof. Dr. Ahmad Zulfaa Mohamed Kassim for his invaluable guidance, insightful supervision and endless encouragement throughout this project. I have gained a lot of knowledge about research techniques and technical writing. Without the guidance and advice from him, this final year project will not be done completely on time.

Apart from that, I would like to express my deepest gratitude to my family, fellow friends and course mate for their endless support and encouragement throughout the time. I would also like to extend my gratitude to all School of Aerospace Engineering staffs for their kind cooperation, willingness in preparing a comfortable environment and facilities.

Once again, I would like to thank all the people, including those who I might have missed out mentioning their names but have helped me directly or indirectly in accomplishment of this project. Thank you very much.

# **ANALYSIS AND COMPARISON OF AIRFOIL-POLAR PREDICTION METHODS FOR VERTICAL-AXIS TURBINES**

## **ABSTRACT**

The numerical method used to analyse the vertical-axis turbine (VAT) performance in this study utilized the lifting line theory coupled with free vortex wake (LLTFVW). This method computes the blade forces from the tabulated airfoil lift and drag coefficients. The rotating axis of the blades of VAT is perpendicular to the wind stream leading to the blade experiencing a wider range of incidence angle than horizontal-axis turbine (HAT). Thus, full-range airfoil data is required to compute the turbine performance of VAT. The polar data can be obtained experimentally, but only for a limited range of angle of attack due to the high experimental costs and the limitations of specific wind turbines. A general approach for the polar extrapolation is applying curve fits generalisation to the experimental measured data. The full-range polar data obtained from QBlade is dependent on the prediction model used, which ultimately affects the simulated performance on the turbine. Hence, the present study had simulated and investigated the accuracy of full-range polar data and its effects on turbine performance through the Viterna and Montgomerie polar-extrapolation techniques in QBlade. This paper also performed optimization tests on the LLT simulation and a validation test with available simulation data to improve the reliability of the simulation data because the parameterization of the LLT simulation in QBlade involves numerous complicated settings. The turbine design used for the simulation is with a single blade of NACA 0018 airfoil. A focus is set on achieving high robustness and computational efficiency. From this study, a good agreement with the experimental and numerical polars data from the literature can be found based on aerodynamic characteristics of airfoil and turbine performance. The simulation results of this study have also been demonstrated to be reliable for future use.

# ANALISIS DAN PERBANDINGAN KAEDAH PREDIKASI AEROFOIL POLAR UNTUK TURBIN PAKSI MENEGAK

## ABSTRAK

Kaedah berangka yang digunakan untuk menganalisis prestasi turbin paksi menegak dalam kajian ini menggunakan *lifting line theory coupled with free vortex wake (LLTFVW)*. Kaedah ini menghitung daya bilah dari pekali lif dan seret. Paksi putaran bilah turbin paksi menegak adalah tegak lurus dengan aliran angin yang menuju ke bilah yang mengalami jarak sudut tuju yang lebih luas daripada turbin paksi mendatar. Oleh itu, data aerofoil dengan darjah penuh 360 diperlukan untuk menghitung prestasi turbin paksi menegak. Data kutub dapat diperoleh secara eksperimen, tetapi hanya untuk jarak serangan yang terhad kerana kos eksperimen yang tinggi dan keterbatasan turbin angin tertentu. Pendekatan umum untuk ekstrapolasi kutub adalah menggunakan keluk yang sesuai dengan generalisasi terhadap data yang diukur dari eksperimen. Data kutub darjah penuh yang diperoleh dari *QBlade* bergantung pada model ramalan yang digunakan, yang akhirnya mempengaruhi prestasi simulasi pada turbin. Oleh itu, kajian ini telah mensimulasikan dan menyelidiki ketepatan data darjah penuh dan kesannya terhadap prestasi turbin melalui teknik ekstrapolasi kutub *Viterna* dan *Montgomerie* dalam *QBlade*. Makalah ujian pengoptimuman pada simulasi *LLT* dan ujian pengesahan dengan data simulasi yang tersedia juga dilakukan untuk meningkatkan kebolehpercayaan data simulasi kerana parameterisasi simulasi *LLT* di *QBlade* melibatkan banyak pengaturan yang rumit. Reka bentuk turbin yang digunakan untuk simulasi adalah dengan satu bilah *NACA 0018*. Salah satu tumpuan ialah untuk mencapai kecekapan komputasi yang tinggi. Dari kajian ini, kesepakatan yang baik dengan data kutub eksperimen dan berangka dari literatur dapat dijumpai berdasarkan ciri-ciri aerodinamik prestasi udara dan turbin. Hasil simulasi kajian ini juga telah terbukti boleh dipercayai untuk kegunaan masa depan.

# TABLE OF CONTENTS

<b>ENDORSEMENT</b> .....	<b>i</b>
<b>DECLARATION</b> .....	<b>ii</b>
<b>ACKNOWLEDGEMENT</b> .....	<b>iii</b>
<b>ABSTRACT</b> .....	<b>iv</b>
<b>ABSTRAK</b> .....	<b>v</b>
<b>TABLE OF CONTENTS</b> .....	<b>vi</b>
<b>LIST OF FIGURES</b> .....	<b>ix</b>
<b>LIST OF TABLES</b> .....	<b>xiv</b>
<b>LIST OF ABBREVIATIONS</b> .....	<b>xv</b>
<b>LIST OF SYMBOLS</b> .....	<b>xvi</b>
<b>CHAPTER 1 INTRODUCTION</b> .....	<b>1</b>
1.1 Motivation .....	1
1.2 Problem Statement.....	3
1.2.1 Accuracy of Prediction Model for Full-range Airfoil Polar.....	4
1.2.2 Complication of Parameterization of LLT Simulation .....	4
1.3 Objectives.....	5
1.4 Scope and Limitations of Study .....	5
1.5 Chapter Outline .....	6
<b>CHAPTER 2 LITERATURE REVIEW</b> .....	<b>8</b>
2.1 Turbine .....	8
2.1.1 Introduction to Vertical-axis Turbines .....	8
2.1.2 Aerodynamics of Vertical-axis turbines.....	10
2.1.2(a) Geometrical Parameters .....	11
2.1.2(b) Operational Parameters.....	13
2.1.2(c) Turbine Aerodynamic Performance .....	15

2.1.3	Full-range Airfoil Polar Extrapolation .....	18
2.1.3(a)	Viterna Approach.....	18
2.1.3(b)	Montgomerie Approach .....	21
2.1.4	Turbine Model.....	22
2.2	Simulation.....	23
2.2.1	QBlade.....	24
2.2.1(a)	Airfoil Design and Analysis .....	24
2.2.1(b)	Polar Extrapolation to <b>360°</b> .....	26
2.2.1(c)	Blade Design and Optimization.....	27
2.2.1(d)	Turbine Definition and Simulation .....	28
2.2.2	Low Order Computational Modeling – LLTFVW.....	31
<b>CHAPTER 3</b>	<b>METHODOLOGY.....</b>	<b>36</b>
3.1	Overview of Research Methodology.....	36
3.2	Design of Simulation .....	37
3.2.1	Turbine Design Specification.....	37
3.2.2	Simulation and Analysis.....	39
3.2.2(a)	Simulation .....	39
3.2.2(b)	Analysis .....	43
3.3	Optimization and Convergence Tests on Parameterization of LLT Simulation .....	44
3.4	Validation of Simulation .....	46
<b>CHAPTER 4</b>	<b>RESULTS AND DISCUSSION .....</b>	<b>48</b>
4.1	Optimization and Convergence Tests on Parameterization of LLT Simulation .....	48
4.1.1	Wake modeling parameters .....	48
4.1.1(a)	Chordal Location of the Angle of Attack of the Blade.....	48
4.1.1(b)	Simulated Wake Length and Its Truncation .....	50
4.1.2	Operational parameters .....	54
4.1.2(a)	Blade Discretization.....	54

4.1.2(b)	Rotor Revolution .....	55
4.1.2(c)	Azimuthal Step Size .....	57
4.1.2(d)	Single and Multi-Polar Data of the Blade.....	59
4.2	Validation of the Results of Simulations.....	61
4.3	Simulation.....	66
4.3.1	Aerodynamic Characteristics of Airfoil Polar.....	66
4.3.1(a)	XFOIL Simulation (Pre-stall Airfoil Polar).....	66
4.3.1(b)	Full-range Airfoil Polar .....	68
4.3.2	Turbine Performance .....	74
4.3.3	Percentage of Difference on Each Performance Variables .....	81
<b>CHAPTER 5</b>	<b>CONCLUSIONS AND RECOMMENDATIONS.....</b>	<b>84</b>
5.1	Conclusions .....	84
5.2	Recommendations for Future Works.....	85
<b>REFERENCES.....</b>		<b>87</b>
<b>APPENDICES .....</b>		<b>93</b>

## LIST OF FIGURES

Figure 1.1: A schematic representation of vertical-axis turbine design's inherent advantage in coping with varying wind direction (Bertényi, Wickins and McIntosh, 2010)...	2
Figure 2.1: Types of vertical-axis turbines (Mohammed <i>et al.</i> , 2020).....	9
Figure 2.2: Darrieus turbines operating principle (E.A.D. Kumara K.G.R.M. Jayathilake, 2017). .....	10
Figure 2.3: Definition of blade pitch angle (Du, Ingram and Dominy, 2019). ....	13
Figure 2.4: Angle of attack at each azimuthal position for different tip-speed ratio (Li <i>et al.</i> , 2021).....	14
Figure 2.5: The components of velocities and forces on a Darrieus vertical-axis turbine. ....	16
Figure 2.6: Detailed view of velocity components on an airfoil at an azimuthal position.....	16
Figure 2.7: Airfoil NACA 0018.....	23
Figure 2.8: Basic software modules inside QBlade (D Marten and Wendler, 2013).....	24
Figure 2.9: Airfoil design module using XFOIL inside QBlade.....	25
Figure 2.10: XFOIL direct analysis module. ....	26
Figure 2.11: Polar Extrapolation to 360°. ....	27
Figure 2.12: Blade design and optimization module.....	28
Figure 2.13: LLTFVW turbine simulation (3D View).....	29
Figure 2.14: LLTFVW turbine simulation (Graph View).....	30
Figure 2.15: LLTFVW turbine simulation operational point settings. ....	30
Figure 2.16: LLTFVW turbine simulation output, algorithm and wake parameters settings. ...	31
Figure 2.17: Illustration of blade panel, the position of lifting line, shed and trailing vortex line elements (Marten, Lennie, <i>et al.</i> , 2016). ....	32
Figure 2.18: Top view of single blade wake at a $\lambda$ of 4 with wake truncation 4,7 and 10 (Marten <i>et al.</i> , 2019).....	33
Figure 2.19: Side view of single blade wake without wake reduction.....	34

Figure 2.20: Side view of single blade wake with wake reduction of 30%. .....	35
Figure 3.1: Flow diagram of the research project on airfoil polar prediction methods.....	36
Figure 3.2: Turbine model simulated from blade design module. ....	38
Figure 3.3: Airfoil design and analysis specification. ....	39
Figure 3.4: Setup of finetuning od decomposition. ....	40
Figure 3.5: Decomposed polar curves using the Viterna polar-extrapolation technique. ....	41
Figure 3.6: Decomposed polar curves using the Montgomerie polar-extrapolation technique. .....	41
Figure 3.7: Downstream wake behind the turbine. ....	43
Figure 4.1: Comparison between various chordal locations used to calculate the angle of attack of the blade.....	49
Figure 4.2: Enlarged view of the comparison between various chordal locations used to calculate the angle of attack of the blade. ....	49
Figure 4.3: Comparison of the momentary thrust coefficient between various chordal locations used to calculate the angle of attack of the blade.....	50
Figure 4.4: Comparison of the angles of attack between various simulated wake length in a revolution based on dataset by Viterna present study.....	51
Figure 4.5: Comparison of the momentary thrust coefficient between various simulated wake length in a revolution based on dataset by Viterna present study.....	51
Figure 4.6: Deviation between various simulated wake length in a revolution based on dataset by Viterna present study.....	52
Figure 4.7: Comparison of the angles of attack between various simulated wake length in a revolution based on dataset by Bianchini et al. (2016). ....	52
Figure 4.8: Comparison of the momentary thrust coefficient between various simulated wake length in a revolution based on dataset by Bianchini et al. (2016). ....	53
Figure 4.9: Deviation between various simulated wake length in a revolution based on dataset by Bianchini et al. (2016). ....	53
Figure 4.10: Comparison of the angles of attack of the blade in a single revolution for five different sets of blade discretization.....	54

Figure 4.11: Comparison of the momentary thrust coefficient of the blade in a single revolution for five different sets of blade discretization.....	55
Figure 4.12: Comparison of the angles of attack between various rotor revolution. ....	56
Figure 4.13: Comparison of the momentary thrust coefficient between various rotor revolution. ....	56
Figure 4.14: Convergence of the average power coefficient of the turbine rotor towards a steady-state value, relative to the simulation time and rotor revolutions.....	57
Figure 4.15: Comparison of the angles of attack of the blade in a single revolution for four different sets of azimuthal step size. ....	58
Figure 4.16: Comparison of the momentary thrust coefficient of the blade in a single revolution for four different sets of azimuthal step size.....	58
Figure 4.17: Comparison of simulation time for four different sets of azimuthal step size.....	59
Figure 4.18: Comparison of the angles of attack and the Reynolds number between single and multi-polar data of the blade. ....	60
Figure 4.19: Comparison of the lift coefficient and the momentary thrust coefficient between single and multi-polar data of the blade.....	60
Figure 4.20: Comparison of the average power coefficient between Marten’s works and present study.....	61
Figure 4.21: Comparison of the momentary torque coefficient between works of Marten et al. and present study at $\lambda = 1.67$ .....	63
Figure 4.22: Comparison of the momentary torque coefficient between works of Marten et al. and present study at $\lambda = 2.2$ .....	64
Figure 4.23: Comparison of the momentary torque coefficient between works of Marten et al. and present study at $\lambda = 3.34$ .....	64
Figure 4.24: Comparison of the momentary torque coefficient between works of Marten et al. and the study at $\lambda = 3.9$ . ....	65
Figure 4.25: Comparison of the momentary torque coefficient between works of Marten et al. and the study at $\lambda = 4.45$ . ....	66

Figure 4.26: Comparison of the lift coefficient of the airfoil from this study and the experimental works in other studies between $-15^\circ$ and $15^\circ$ .....	67
Figure 4.27: Comparison of the drag coefficient of the airfoil from this study and the experimental works in other studies between $-15^\circ$ and $15^\circ$ .....	68
Figure 4.28: Airfoil lift coefficient data extrapolated with Viterna and Montgomerie techniques. ....	69
Figure 4.29: Airfoil drag coefficient data extrapolated with Viterna and Montgomerie techniques.....	69
Figure 4.30: Comparison of the lift coefficient of the airfoil from this study and the numerical literature between $-180^\circ$ and $180^\circ$ .....	70
Figure 4.31: Comparison of the drag coefficient of the airfoil from this study and the numerical literature between $-180^\circ$ and $180^\circ$ .....	72
Figure 4.32: Comparison of the full-range lift coefficient of the airfoil from this study, the experimental works and the numerical literature. ....	73
Figure 4.33: Comparison of the full-range drag coefficient of the airfoil from this study, the experimental works and the numerical literature. ....	73
Figure 4.34: Comparison of the angle of attack against the azimuthal position of LLT simulation. ....	75
Figure 4.35: Enlarged view of the airfoil lift coefficient data between $-10^\circ$ and $20^\circ$ .....	76
Figure 4.36: Enlarged view of the airfoil drag coefficient data between $-10^\circ$ and $20^\circ$ .....	76
Figure 4.37: Comparison of the Reynolds number against the azimuthal position of LLT simulation. ....	77
Figure 4.38: Comparison of the lift coefficient of turbine blade against the azimuthal position of LLT simulation. ....	79
Figure 4.39: Comparison of the drag coefficient of turbine blade against the azimuthal position of LLT simulation. ....	79
Figure 4.40: Comparison of the lift to drag ratio of turbine blade against the azimuthal position of LLT simulation. ....	80

Figure 4.41: Comparison of the momentary thrust coefficient of turbine blade against the azimuthal position of LLT simulation.....80

## LIST OF TABLES

Table 2.1: Summary of experimental and numerical airfoil polar data used for investigation.	23
Table 3.1: Turbine model design specification. ....	37
Table 3.2: Polar decomposition fine-tuning parameters' denifition. ....	40
Table 3.3: LLT simulation parameters. ....	42
Table 3.4: LLT simulation parameters chosen for optimization. ....	44
Table 3.5: LLT simulation parameters for optimization & convergence tests.....	45
Table 3.6: Optimization and convergence testing range. ....	45
Table 3.7: Turbine model specifications for validation simulation	46
Table 3.8: LLT simulation parameters for validation simulation. ....	46
Table 4.1: Percentage of difference between each variable for experimental polar data.....	81
Table 4.2: Percentage of difference between each variable for numerical polar data. ....	82

## LIST OF ABBREVIATIONS

AOA	Angle of attack
BEM	Blade element momentum
CFD	Computational Fluid Dynamics
DMS	Double multiple streamtube
HAT	Horizontal-axis turbine
LLTFVW	Lifting-line theory free vortex wake
RANS	Reynolds Averaged Navier-Stokes
VAT	Vertical-axis turbine

## LIST OF SYMBOLS

$C_D$	: Turbine blade drag coefficient
$C_L$	: Turbine blade lift coefficient
$C_N$	: Normal force coefficient
$C_T$	: Tangential force coefficient
$C_d$	: Airfoil drag coefficient
$C_l$	: Airfoil lift coefficient
$C_m$	: Moment coefficient
$C_p$	: Power coefficient
$C_t$	: Momentary thrust coefficient
$C_\tau$	: Momentary torque coefficient
$F_{Ta}$	: Average tangential force [N]
$U_\infty$	: Free stream velocity [m/s]
$U_a$	: Induced velocity [m/s]
$U_c$	: Chordal velocity component [m/s]
$U_n$	: Normal velocity component [m/s]
$h$	: Blade height [mm]
$AR$	: Turbine aspect ratio
$D$	: Turbine rotor diameter [mm]
$L/D$	: Turbine lift-to-drag ratio
$P$	: Power output [W]
$Q$	: Total torque [Nm]
$S$	: Blade swept area [m <sup>2</sup> ]
$W$	: Relative stream velocity [m/s]
$c$	: Blade chord length [mm]
$f$	: Transformation function

$n$	: Number of blades
$r$	: Rotor radius [ $mm$ ]
$s$	: Separated flow
$t$	: Attached flow
$\nu$	: Kinematic viscosity of air [ $m^2/s$ ]
$\alpha$	: Angle of attack [ $^\circ$ ]
$\beta$	: Blade pitch angle [ $^\circ$ ]
$\theta$	: Azimuthal position [ $^\circ$ ]
$\lambda$	: Tip-speed ratio
$\rho$	: Density of air [ $kg/m^3$ ]
$\sigma$	: Solidity
$\omega$	: Turbine rotational speed [ $m/s$ ]
$l_w$	: Simulated wake length
$Rev$	: Rotor revolution

# CHAPTER 1

## INTRODUCTION

This chapter introduces the motivation of this research project on vertical-axis turbines and the current research problems on its development. A software to simulate vertical-axis turbines performance is presented and this research project's primary goal is defined in detail.

### 1.1 Motivation

The rapid growth of urbanization has led to an escalation in demand for energy (Ishugah *et al.*, 2014). The research on various energy conversion to electrical energy is very significant worldwide, especially in urban area. The nature of wind in the urban area is characterised by low annual mean wind speeds and irregular turbulent winds that occur in the atmospheric boundary layer. The turbulent flow is due to uneven ground topography or barriers when the wind interacts with them. Thus, the complicated urban wind resources cause rapid changes in wind direction and magnitude (KC, Whale and Urnee, 2019). Horizontal-axis turbine (HAT) and vertical-axis turbine (VAT) are two common types of turbines. Horizontal-axis turbines are relatively less efficiency in urban wind condition due to yaw misalignment (Whittlesey, 2017). Compared to a horizontal-axis one, vertical-axis turbines have better performance as theoretically they are less susceptible to the changes in wind direction as shown in Figure 1.1 (Bertényi, Wickins and McIntosh, 2010; Du, Ingram and Dominy, 2019). Vertical-axis turbines have several distinct advantages: simple blade shape design, low aerodynamic noise and ease of maintenance (Kumar, Raahemifar and Fung, 2018). In the past, they drew far less interest in research purposes. This is due to aerodynamics' complexity due to variations in angles of attack and relative velocity throughout each turbine revolution

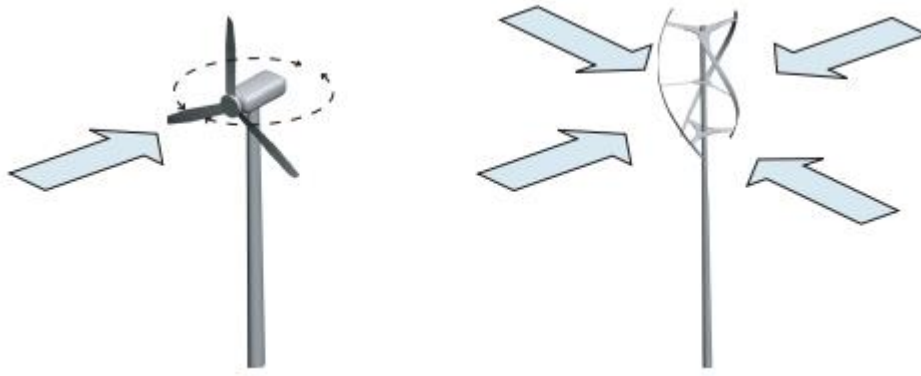


Figure 1.1: A schematic representation of vertical-axis turbine design's inherent advantage in coping with varying wind direction (Bertényi, Wickins and McIntosh, 2010).

Recently, many experimental and numerical investigations have been performed on the aerodynamics of vertical-axis turbines, but their performance remains unsatisfactory and there is still potential for improvement. Based on Roy *et al.* (2017), since vertical-axis turbine blades undergo a wide range of incidence angles than horizontal-axis turbine blades, parametric investigation on a wide range of vertical-axis turbine designs is a costly and time-consuming process. As a result, the Blade element momentum (BEM) model is used for numerical analysis due to its utility in predicting the performance of vertical-axis turbines in a crude but reasonably accurate manner. However, the BEM model becomes invalid in simulations with a high tip speed ratio and high rotor solidity because the momentum equations are insufficient in this case (Islam, 2008). The most apparent problems in the BEM theory are that the predicted findings are less than the measured maximum power, and there is a quick reduction in turbine power after stall (Viterna and Janetzke, 1982). The Reynolds Averaged Navier-Stokes (RANS) method in computational fluid dynamics (CFD) has been used to evaluate and optimise turbine efficiency. In comparison to momentum modeling, however, CFD is not user-friendly and has a high computational cost. Various approaches, such as the double multiple streamtube (DMS) model, vortex model, and cascade model, were also introduced to predict turbine output, especially vertical-axis turbines performance (Du, 2015). The DMS model and the Lifting Line

Theory coupled to a free vortex wake (LLTFVW) model are two computationally efficient low order models capable of capturing specific unsteady characteristics in vertical-axis turbines.

In 2010, the QBlade software project was created as an open-source platform for wind turbine simulation and design. It used the BEM model to simulate the horizontal-axis turbines and DMS algorithms and the LLTFVW model to simulate vertical-axis turbines performance. This single tool provides all of the features required to design and simulate aerodynamic wind turbines, and eliminate the need to import, convert or process data from other sources (D Marten and Wendler, 2013). It is more user-friendly than CFD simulation because it is embedded in a simple graphical user interface, making it more accessible than comparable simulation codes. This project will utilize QBlade software for both airfoil and turbine simulation. The study of 360° airfoil polar extrapolation will be performed out using the embedded Viterna and Montgomerie approaches to code. Even though it is open source, the computational findings are not entirely reliable. Thus, the research on determining the accuracy and reliability of the computational results predicted with QBlade by comparing them to experimental and numerical data is still ongoing.

## **1.2 Problem Statement**

The numerical analysis methods DMS and LLTFVW compute blade forces using the airfoil's tabulated lift and drag coefficients. Vertical-axis turbines blades require a full-range of airfoil polar data to calculate the turbine output due to its rotating axis is perpendicular to the wind stream. The accuracy of these models can readily be influenced by how closely the tabular data corresponds to the actual aerodynamic performance of the airfoils in motion of a Darrieus rotor (Marten, Bianchini, *et al.*, 2016). The problem statements in this study are presented as below:

- a. The full airfoil polar data obtained from QBlade is dependent on the prediction model used, which ultimately affects the simulated performance on turbine.
- b. The parameterization of the LLT simulation in QBlade involves numerous complicated settings which affect the reliability of the simulated data.

### **1.2.1 Accuracy of Prediction Model for Full-range Airfoil Polar**

The airfoil polar data for the deep stall and beyond are often more challenging to obtain than data near  $0^\circ$  angle of attack. Thus, investigating the physical structure of wind turbines in terms of polar extrapolation of airfoil data has become more challenging. These vertical-axis turbines modeling techniques are very sensitive to minor variations in input data of blade forces, and it is therefore crucial for the post-stall airfoil data to be accurate (Rainbird, Peiro and Graham, 2017). The full-range airfoil polar data typically can be obtained experimentally. However, due to high experimental costs and the limitations of specific wind tunnels, it can only be done for a narrow range of angles of attack. The polar extrapolation aims is to predict the airfoil's post-stall aerodynamic characteristics, which are then further analysed to determine the data's reliability. Therefore, the general approach for obtaining the full-range airfoil polar data is to apply curve fit generalisation to experimentally measured data. Several semi-empirical methods have been developed over the years, such as Viterna-Corrigan (Viterna and Janetzke, 1982), Montgomerie (Montgomerie, 2004), Kirke (Bianchini, Balduzzi, Rainbird, *et al.*, 2016), and Spera (Spera, 2010). However, none has been identified as the most accurate method over a wide range of applications (Truong, 2020). The Viterna and Montgomerie approaches, integrated into QBlade, are the most extensively used methods for airfoil polar extrapolation. As a result, they have been chosen to be studied in this research.

### **1.2.2 Complication of Parameterization of LLT Simulation**

It is important to note that very accurate polar and proper dynamic stall sub-models must be used to show a very high accuracy turbine simulation that is reliable to the actual

performance of vertical-axis turbines (Ferreira *et al.*, 2007; Bianchini, Balduzzi, Ferrara, *et al.*, 2016). It has only been five years since the LLT module was implemented in QBlade. There are only limited studies on LLT simulation in QBlade that can be utilised to set up the simulation parameters appropriately. Thus, the reliability of turbine simulation data by tweaking the simulation settings is also crucial in this study.

### **1.3 Objectives**

A list of tasks must be completed in order to address the problem statements described in section 1.2. The following are the objectives that must be met to reach the investigation's goal.

- a. To simulate and investigate the accuracy of full-range airfoil polar data and its effects on turbine performance through QBlade.
- b. To perform optimization tests on the LLT simulation and a validation test with available simulation data to improve the reliability of the simulation data.

The full-range airfoil polar data will be analysed and extrapolated using the QBlade software's polar extrapolation module, and data from other research studies will be compared. Different sets of full-range airfoil polar data will be used in the LLT simulation to study the influence of airfoil polar data on turbine performance.

The LLT simulation parameters will be optimised to find the best settings for obtaining the most trustworthy results for investigation purposes. To assure the reliability of QBlade software simulation, a validation test based on available research studies will be conducted.

### **1.4 Scope and Limitations of Study**

This study focuses on the full-range airfoil polar and the LLT simulation. The pre and post-stall aerodynamic performance of airfoil are investigated through the lift and drag

coefficient variables, while the turbine performance is investigated through a single rotor blade turbine model. The effects of airfoil aerodynamic performance of the turbine performance are observed. The airfoil chosen for this study was NACA 0018 because it is a symmetrical airfoil that was commonly used during the early stages of vertical-axis turbines development due to readily available test data suitable for aviation purposes (Mohan Kumar *et al.*, 2019). It is ideal for vertical-axis turbines where the angles of attack of rotor blades changed constantly. Many research papers include the aerodynamic performance of NACA 0018, which are useful for the investigation of this study. In recent years, several studies have concentrated on studying vertical-axis turbines with thicker profiles, which have the advantage of a wider range of pre-stall angles of attacks. As stated in Ionescu *et al.* (2015), the stall angle is determined by the profile thickness and the curvature of the leading edge. Thus, the analysis was based on the aerodynamic performance of NACA 0018, which is more comprehensive enough and has good lift-drag properties. All simulations will be conducted through QBlade software with data post-processing done in Matlab. Various optimization tests are also performed to enhance the simulation performance. This study also includes a validation test based on available LLT simulation data.

## **1.5 Chapter Outline**

The thesis is organized into the following five chapters: Chapter 1 (Introduction), which introduced the motivation and an overview of this study. The literature of aerodynamics of vertical-axis turbines, the full-range airfoil polar extrapolation approach, the blade profile (NACA 0018), and QBlade software are described in detail in Chapter 2 (Literature Review). In Chapter 3 (Methodology), the design of simulation includes those optimization and convergence tests for simulation that has be completed are presented in this chapter. The approach for simulation reliability tests using available research is also defined. The findings

of the airfoil and turbine rotor simulations are covered in Chapter 4 (Results and Discussion). The effects of full-range airfoil polar on the turbine performance are investigated and addressed. This chapter also contains the results of simulation validation. The final chapter, Chapter 5 (Conclusions and Recommendations) will summaries of the findings of this study, and the conclusions and recommendations for future work are also be reviewed.

## **CHAPTER 2**

### **LITERATURE REVIEW**

This chapter presents the literature relevant to the simulation of lift-driven vertical-axis turbines. Turbine and simulation are the two primary aspects of the literature. The turbine section is described into three subsections: the introduction to vertical-axis turbines, full-range airfoil polar extrapolation approach, and turbine model. While the QBlade software and the LLTFVW model are two subsections in the simulation section.

#### **2.1 Turbine**

The straight-blade (H-Darrieus) vertical-axis wind turbine is the subject of this research study. This section mainly explains the principle of vertical-axis turbines, full-range polar extrapolation approach, and a turbine model with blades profile using the NACA 0018 airfoil. The development of vertical-axis turbines is introduced in the first subsection. Next, the aerodynamics of vertical-axis turbines are described, followed by the turbine aerodynamic performance expressed in mathematical expressions.

##### **2.1.1 Introduction to Vertical-axis Turbines**

Vertical-axis windmills were the first practical wind devices documented in historical papers. These windmills had multi-bladed rotors and operated at relatively low tip-speed ratio  $\lambda$ , explaining their inefficiency (Li, 2020). The first vertical-axis turbines were a simple device. A French aeronautical engineer named Georges Jean Marie Darrieus invented the first lift-based vertical-axis turbines in the 1920s and patented in the US in 1931 (Sidén, Ambrosio and Medaglia, 2010). There are two main types of vertical-axis turbines: drag-driven vertical-axis turbines (Savonius type) and lift-driven vertical-axis turbines (Darrieus type), as shown in Figure 2.1. The Darrieus-type vertical-axis turbines were patented in two rotors: the curved blade (Darrieus type) and the straight blade (H-Darrieus type). This study focused on the H-

Darrieus-type vertical-axis turbines, which are point of interest for their advantages of simple design, low cost, and good efficiency (Li, 2020). Darrieus turbines' efficiency ranges from 30% to 40 %, which is just slightly lower than horizontal-axis turbines, which ranges from 40% to 50%.

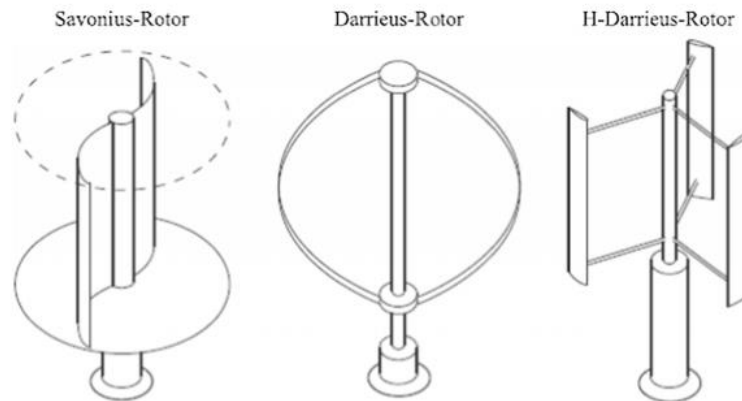


Figure 2.1: Types of vertical-axis turbines (Mohammed *et al.*, 2020).

The working principle of Darrieus vertical-axis turbines is that when its blade is operating, it moves in a circular motion through the air, as illustrated in Figure 2.2. When the wind flows around the turbine, it creates a suction on the front side of the turbine, which drives the blades to rotate. This movement enhances the blade's rotation in the direction in which it is already moving. Vertical-axis turbines usually operate at a lower  $\lambda$  compared to horizontal-axis turbines, and yet the operation of vertical-axis turbines creates lower noise. The noise can be separated into aerodynamic and mechanical noise. The aerodynamic noise is originated as the air flows around the blade and derives from numerous complex flow phenomena. It normally increases with tip speed, therefore the most sound is produced at or around the blade's tip. While the relative motions of mechanical components in the gearbox, generator, yaw drives, cooling fans, hydraulics, and power electronics cause mechanical noise (Möllerström *et al.*, 2014). The only drawbacks of vertical-axis turbines are that in some cases it is not self-starting and needs a motor to get the rotor started. The electricity to the motor is shut off as the blade speed increases, and it begins to act as a generator.

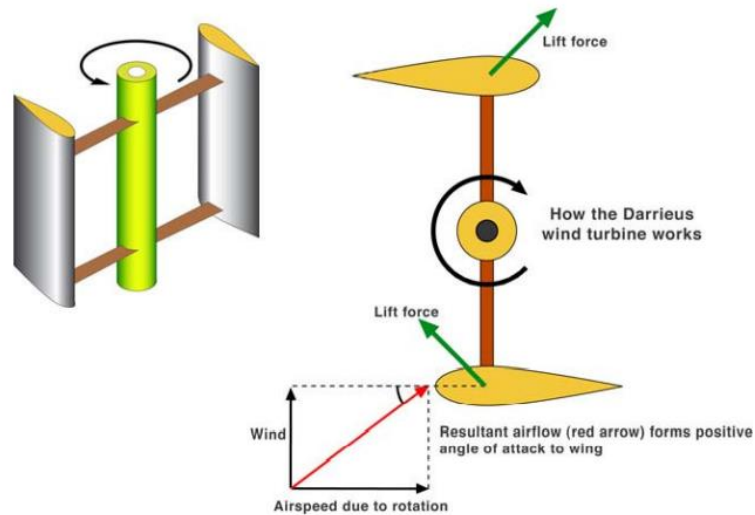


Figure 2.2: Darrieus turbines operating principle (E.A.D. Kumara K.G.R.M. Jayathilake, 2017).

The Darrieus turbines are currently applicable in terms of an off-grid decentralised power generation such as the grid monitoring telecommunication station in South Korea and China, wind and solar lamps, and polar research system power supply in Antarctica. They can also generate decentralised electricity on the grid, such as energy recovery systems, energy supply on rooftops in metropolitan areas, and wind farms (Co, Business and Nations, 2015). In addition, because the wind conditions on the roadway are more conducive to vertical-axis turbines, they have recently been deployed as highway power generation (Bidi *et al.*, 2017).

### 2.1.2 Aerodynamics of Vertical-axis turbines

The performance of the vertical-axis turbines is affected by the geometrical and operational characteristics. The geometrical parameters are the design specification of the turbine and its blades, whereas the operational parameters are the turbine's operation and wind condition. The turbine's performance is computed through a set of mathematical expressions and illustrated with schematic diagrams.

### 2.1.2(a) Geometrical Parameters

(i) Number of blades,  $n$

Vertical-axis turbines for small-scale home use typically have three blades, which is an optimal number of blades. Since the number of blades can counteract aerodynamics loads, they have a significant impact on the smoothness of rotor operation (Castillo, 2011). The addition of an extra blade reduces the maximum loads generated by the turbine while increasing the frequency response of these loads. The torque, thrust, and lateral force ripples are greatly reduced when the number of blades is increased from two to three with constant solidity, but similar power curves are observed (Li *et al.*, 2015; Delafin *et al.*, 2016). The use of three or even four blades appear to be significant enough to increase the turbine's design life.

(ii) Solidity,  $\sigma$

Solidity significantly impacts turbine performance, altering the power coefficient,  $C_p$  variation with  $\lambda$ , the turbine's maximum efficiency, and its ability to self-start (Du, Ingram and Dominy, 2019). It is defined as the blade area ratio to the turbine's swept area as represented in Eqs. (2.1), where  $n$  is the number of blades,  $c$  is the chord length and  $D$  is the diameter of the turbine.

$$\sigma = \frac{nc}{D} \quad (2.1)$$

The desirable range of solidity values for Troposkien-darrieus vertical-axis turbines should be between 0.2 to 0.25, ranging between 0.1 to 0.2 for H-Darrieus vertical-axis turbines (Hameed and Afaq, 2013). The value of solidity is preferred to be low for three or more blades of vertical-axis turbines that operate at high  $\lambda$ . The output power of an optimal turbine solidity would be maximized, with the optimal value depending on the operational conditions.

(iii) Blade airfoil profile

Symmetrical airfoils such as NACA 0012, 0015, and NACA 0018 are widely used in small vertical-axis turbines because they produce the same lift and drag characteristics on both the upper and lower surfaces (Bedon, De Betta and Benini, 2016). As a result, the airfoils provide lift from both sides of the airfoil during the turbine rotation. These profiles have been well-studied, and data for a wide range of conditions are readily available, making aerodynamic design and theoretical power prediction relatively simple. However, no recent study has concluded that symmetrical airfoils are the most efficient for vertical-axis turbines. The other airfoil parameters, such as thickness and camber, will also significantly impact vertical-axis turbines' aerodynamic performance.

(iv) Turbine aspect ratio,  $AR$

The turbine aspect ratio is defined as the ratio between the blade height,  $h$ , and rotor radius,  $R$ , as presented in Eqs. (2.2). The power efficiency of a wind turbine is affected by the aspect ratio chosen. The aspect ratio influences the Reynolds number,  $Re$  and as a result, the power coefficient. Based on the findings of Brusca *et al.* (2014), a lower aspect ratio turbine has several advantages compared to one with a higher value, such as producing a higher power coefficient, a structural advantage by having a thicker blade, and a more excellent in-service stability from the greater inertia moment of the turbine rotor. However, an optimal value of aspect ratio should be chosen based on the environmental condition that the turbine experiences.

$$AR = \frac{h}{R} \quad (2.2)$$

(v) Blade pitch angle,  $\beta$

The blade pitch angle is compelling for vertical-axis turbines performance optimization because it is simple to implement in practice and does not incur high manufacturing, installation, or maintenance costs. The general definition of blade pitch angle is illustrated in Figure 2.3. When the blade nose in is a positive pitch ( $\beta$ ) and nose out is negative pitch ( $-\beta$ ).

According to Rezaeiha *et al.* (2017), variable blade pitch angle can enhance the vertical-axis turbines' performance. A positive blade pitch angles result in a higher moment coefficient,  $C_m$  only over a small part of the revolution due to variations in the angle of attack (AOA) during the turbine revolution.

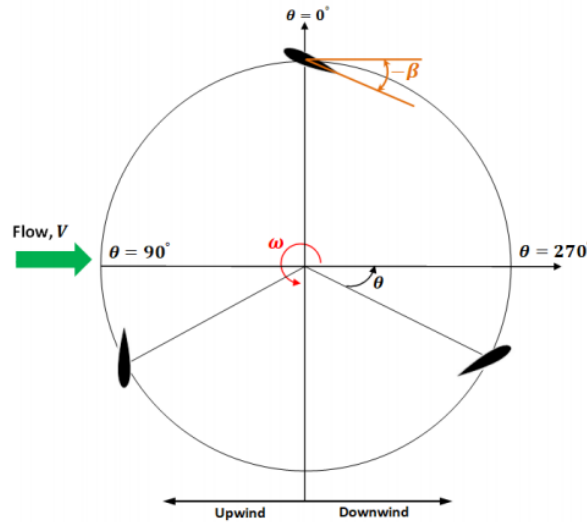


Figure 2.3: Definition of blade pitch angle (Du, Ingram and Dominy, 2019).

### 2.1.2(b) Operational Parameters

#### (i) Tip-speed ratio, $\lambda$

Tip-speed ratio (TSR) is defined as the ratio between the rotational speed of the blade tip and the actual wind velocity as presented in Eqs. (2.3), where  $R$  is the turbine radius,  $\omega$  is the turbine rotational speed, and  $U_\infty$  is the free stream velocity.

$$\lambda = \frac{R\omega}{U_\infty} \quad (2.3)$$

The value of  $\lambda$  affects the range of variations of angle of attack on blades during each turbine revolution, as shown in Figure 2.4. A low  $\lambda$  value will correspond to a large variety of angles of attack that the turbine will experience. Consequently, the turbine will face flow separation and resulting power loss if the stall angle is exceeded. When a dynamic stall occurs, there should be a stall correction for aerodynamic loads. However, this correction is not required

at high  $\lambda$  because the dynamic stall is avoided. Thus, an optimal value of  $\lambda$  should be applied to optimise turbine performance.

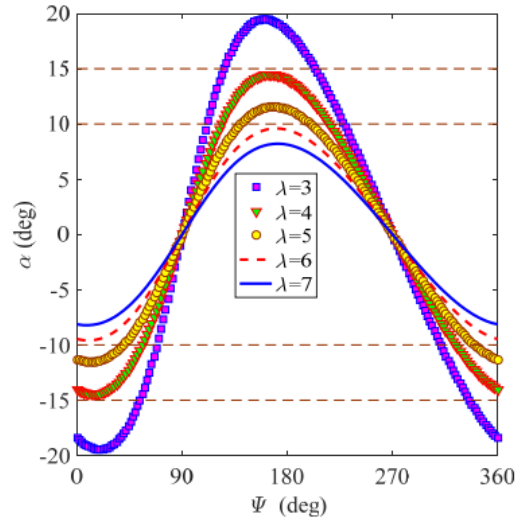


Figure 2.4: Angle of attack at each azimuthal position for different tip-speed ratio (Li *et al.*, 2021).

(ii) Reynolds number,  $Re$

The flow development over the blades, which have an airfoil cross-section, is critical to the performance of VAWTs. Compared to static airfoils, the existence of the two sources of unsteadiness, angle of attack and relative velocity, causes considerable changes in boundary layer events (Dumitrache, Dumitrescu and Frunzulica, 2013). The effect of Reynolds number on dynamic stresses on blades and turbine performance cannot be easily deduced from static airfoil knowledge and necessitates a specific investigation. The Reynolds number is a measure of the viscous behavior of air as formulated in Eqs. (2.4), where  $U_\infty$  is the relative wind velocity,  $c$  is the blade chord, and  $\nu$  is the kinematic viscosity of air.

$$Re = \frac{U_\infty c}{\nu} \sqrt{1 + (TSR)^2} \quad (2.4)$$

(iii) Turbulence intensity

Turbulence is a complicated process that can have a significant impact on wind turbine output (Wekesa *et al.*, 2016). Turbulence intensity is defined as the ratio of the standard deviation of fluctuating wind velocity to the mean wind speed, and it also represents the

intensity of wind velocity fluctuation. It is critically valuable for small wind turbines. Based on Spera (2010) and Wu *et al.* (2020), the turbine still has greater power efficiency with higher turbulence, implying that the H-rotor is ideally suited to wind locations with turbulent winds. Several studies have attempted to characterize the influence of wind turbulence on wind turbines. The turbulence effect on wind turbine performance in an urban context is affected by turbulence intensity and the size of turbulence scales. Similar to other operational parameters, an optimal value of turbulence intensity should be used based on the wind condition to obtain the best turbine performance. However, according to the findings Siddiqui *et al.* (2015), increasing turbulence intensity from 5% to 25% reduces wind turbine performance by around 23% to 42% compared to no turbulence in the incoming wind field for an offshore vertical-axis wind turbine.

### **2.1.2(c) Turbine Aerodynamic Performance**

The general mathematical expression that described the aerodynamic models must be clearly understood before comparative analysis of the turbine performance is done. The turbine performance is determined based on its power generation, which is governed by those geometrical and operational parameters that have been discussed in section 1.1.1(b)(i) and (ii). The aerodynamic characteristics of vertical-axis turbines are illustrated in a two-dimensional diagram, as shown in Figure 2.5. The detailed view of the velocity component on an airfoil at an azimuthal position is presented in Figure 2.6. There is a free stream velocity,  $U_\infty$ , which is the wind flow toward the turbine rotor from the left side. The relative stream velocity,  $W$  is the flow toward the airfoil at each azimuthal position. It can be obtained from the chordal velocity component,  $U_c$ , and the normal velocity component,  $U_n$ , which are written as in Eqs. (2.5), Eqs. (2.6) and Eqs. (2.7).

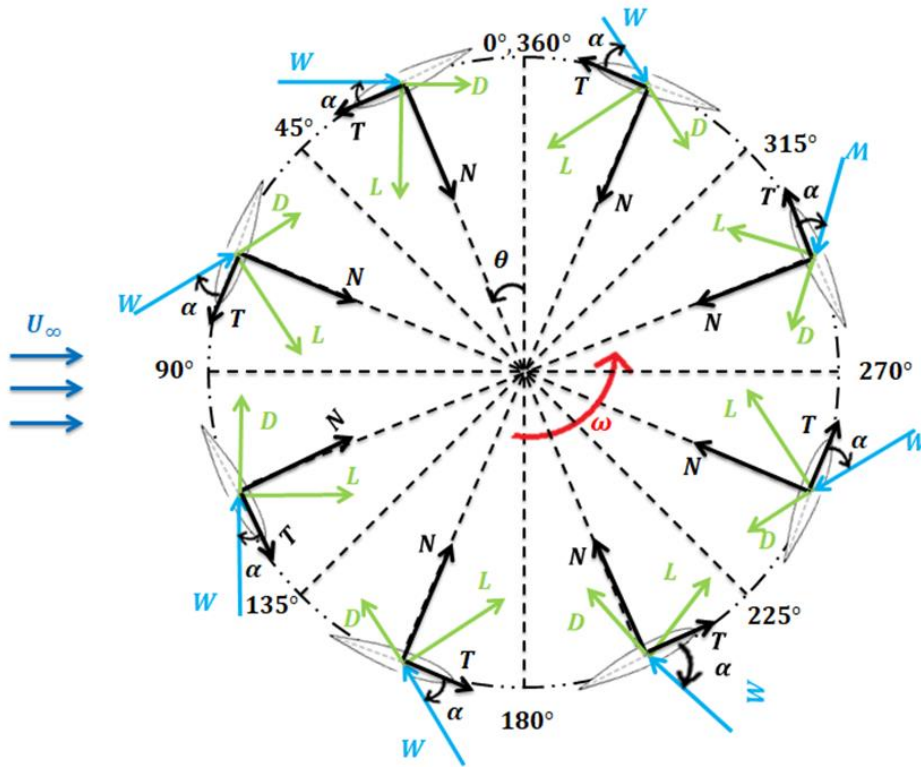


Figure 2.5: The components of velocities and forces on a Darrieus vertical-axis turbine.

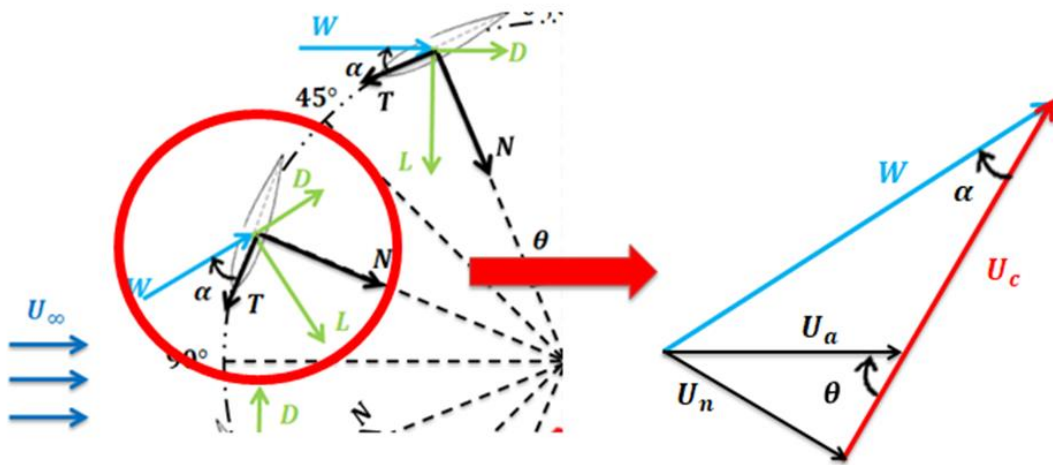


Figure 2.6: Detailed view of velocity components on an airfoil at an azimuthal position.

$$U_c = R\omega + U_a \cos\theta \quad (2.5)$$

$$U_n = U_a \sin\theta \quad (2.6)$$

$$W = \sqrt{U_c^2 + U_n^2} \quad (2.7)$$

We can also find the dimensionless velocity ratio as shown in Eqs. (2.8) by inserting Eqs. (2.5) and Eqs. (2.6) into Eqs. (2.7). It is critical to comprehend how the angle of attack,  $\alpha$ , changes with respect to the relative stream velocity and is expressed as in Eqs. (2.9).

$$\frac{W}{U_\infty} = \frac{W}{U_a} \cdot \frac{U_a}{U_\infty} = \frac{U_a}{U_\infty} \sqrt{\left[ \left( \frac{R\omega}{U_\infty} / \frac{U_a}{U_\infty} \right) + \cos\theta \right]^2 + \sin^2\theta} \quad (2.8)$$

$$\alpha = \tan^{-1} \left( \frac{U_n}{U_c} \right) \quad (2.9)$$

By inserting Eqs. (2.5) and Eqs. (2.6) into Eqs. (2.9), and non-dimensionalizing, we obtained Eqs. (2.10).

$$\alpha = \tan^{-1} \left( \frac{\sin\theta}{(R\omega/U_\infty)/(U_a/U_\infty) + \cos\theta} \right) \quad (2.10)$$

The changes on the relative stream velocity have resulted in variations in lift and drag forces and the forces produced at each azimuthal position,  $\theta$ . The lift and drag forces are then nondimensionalised by dividing through dynamic pressure to obtain lift coefficient,  $C_L$  and drag coefficient,  $C_D$ . The tangential force coefficient,  $C_T$  and the normal force coefficient,  $C_N$  are tabulated from the coefficient of lift and drag. The formulae are expressed in Eqs. (2.11), Eqs. (2.12), Eqs. (2.13), and Eqs. (2.14).

$$C_L = L/0.5\rho W^2 S \quad (2.11)$$

$$C_D = D/0.5\rho U_\infty^2 S \quad (2.12)$$

$$C_T = C_L \sin\alpha - C_D \cos\alpha \quad (2.13)$$

$$C_N = C_L \cos\alpha + C_D \sin\alpha \quad (2.14)$$

The net tangential force and normal force can be described as in Eqs. (2.15) and Eqs. (2.16), and they are treated as a function of azimuthal angle. On a single blade, the average tangential force,  $F_{Ta}$ , can be defined as in Eqs. (2.17).

$$T = C_T \left( \frac{1}{2} \rho c H W^2 \right) \quad (2.15)$$

$$N = C_N \left( \frac{1}{2} \rho c H W^2 \right) \quad (2.16)$$

$$F_{Ta} = \frac{1}{2\pi} \int_0^{2\pi} T(\theta) d\theta \quad (2.17)$$

The total torque,  $Q$  for the number of blades is formulated from the average tangential force as expressed in Eqs. (2.18) and the power output,  $P$ , is shown in Eqs. (2.19).

$$Q = n F_{Ta} R \quad (2.18)$$

$$P = Q \times W \quad (2.19)$$

### 2.1.3 Full-range Airfoil Polar Extrapolation

In this study, the full-range airfoil polar data has been investigated through two approaches, Viterna and Montgomerie. The airfoil polar data have also been further analyzed and compared with available experimental and numerical data, which will be presented in Chapter 4.

#### 2.1.3(a) Viterna Approach

The first study on this technique titled was published in January (Viterna and Corrigan, 1982). Another research that formulated and modified based on the blade element-momentum theory to investigate the theoretical and experimental power from large horizontal axis wind turbines is published later (Viterna and Janetzke, 1982).

The experimental results were found to be in good agreement with the proposed empirical corrections to the aerodynamic characteristics and momentum theory. The power output versus wind speed at a low  $\lambda$  shows the most noticeable improvement with this correction. The empirical correction is by increasing maximum lift and lower drag resulting by using smooth airfoil features, resulting in maximum power. The smooth airfoil data is recommended to analyze the wind turbine rotor performance near the stall.

The drawback of this correction is that it does not improve the rapid decrease in power after stall. Therefore, to increase the correlation between measured and calculated performance, an idealized stall model was applied. It is based on performance that is comparable to the measured data. There are three conditions assumed in this model: (1) The continuity of the stalled and unstalled characteristics at the stall angle, (2) the constant power or torque coefficient after the stall, and (3) at a given blade aspect ratio, the correction on drag coefficient at  $90^\circ$  of the angle of attack. As a result, the calculated polar data values are reflected for  $\alpha > 90^\circ$  and  $\alpha < \alpha_{min}$  (Viterna and Corrigan, 1982).

Equations (2.20) and (2.21) are two formulations for the lift and drag characteristics after stall that satisfy the conditions described above (Viterna and Corrigan, 1982; Viterna and Janetzke, 1982)):

$$C_L = A_1 \sin 2\alpha + A_2 \frac{\cos^2 \alpha}{\sin \alpha} \quad (2.20)$$

$$C_D = B_1 \sin^2 \alpha + B_2 \cos \alpha \quad (2.21)$$

where

$$A_1 = \frac{B_1}{2} \quad (2.22)$$

At the angle of attack of  $90^\circ$ , Eqs. (2.21) expressed as Eqs. (2.23)

$$B_1 = C_{D_{MAX}} \quad (2.23)$$

$C_{D_{MAX}}$  is the drag coefficient at the angle of attack of  $90^\circ$ .  $C_{D_{MAX}}$  for a finite aspect ratio blade is defined as Eqs. (2.24) and yet  $A_1$  can be simplified as Eqs. (2.25).

$$C_{D_{MAX}} = 1.11 + 0.18 AR \quad (2.24)$$

$$A_1 = \frac{C_{D_{MAX}}}{2} \quad (2.25)$$

By rearranging Eqs. (2.20) and Eqs. (2.21), we obtained Eqs. (2.26) and Eqs. (2.27).

$$A_2 = (C_L - C_{D_{MAX}} \sin \alpha \cos \alpha) \frac{\sin \alpha}{\cos^2 \alpha} \quad (2.26)$$

$$B_2 = \frac{C_D - C_{D_{MAX}} \sin^2 \alpha}{\cos \alpha} \quad (2.27)$$

Equations. (2.26) and (2.27) are solved for the stall angle condition for the continuity with the pre-stall airfoil data, and they are expressed in Eqs. (2.28) and Eqs. (2.29).

$$A_2 = (C_{L_S} - C_{D_{MAX}} \sin \alpha_S \cos \alpha_S) \frac{\sin \alpha_S}{\cos^2 \alpha_S} \quad (2.28)$$

$$B_2 = C_{D_S} \frac{C_{D_{MAX}} \sin^2 \alpha_S}{\cos \alpha_S} \quad (2.29)$$

The aspect ratio,  $AR$  in Eqs. (2.24) is obtained from BEM method application where finite blade length will affect the flat plate assumption. The value of  $AR$  for most computations is between the range of 9 to 10. However, the impact of  $AR$  is not significant to the final computational results (Mahmuddin, 2016).

### 2.1.3(b) **Montgomerie Approach**

Montgomerie polar extrapolation approach was established by utilizing the general method proposed which was applying curve fit generalization to the measured data. Thin plate theory (complete stall) complemented with the linear range behavior (potential flow model) is the theory used in this approach (Montgomerie, 2004). The fundamental assumption is that the steady-state and unstable aerodynamics tables can be used together, and the steady-state values are improved with latter effects. Using this latter effect, the elastic behavior of the whole wind turbine is examined in response to gravity and different wind conditions.

The validation of the aerodynamics table in the complete range of angle of attack requires an actual application of aerodynamic code within aeroelastic programs. The latter are typically employed to analyze the entire wind turbine's elastic behavior in response to gravity loading and varying wind conditions. The flow condition before the stall angle behaves very much like a potential flow which is attached flow labelled as  $t$ . While the after-stall flow condition on the suction side of the airfoil is separated flow labelled as  $s$ , a non-potential flow produces a substantial drag force. The blade behaves much like a thin plate with a sharp leading edge in the situation of separated flow. A transformation function,  $f$  is introduced to interpolate between the curves for attached flow ( $f = 1.0$ ) and fully separated flow ( $f = 0$ ) to yield the  $C_L$  curve as expressed in Eqs. (2.30) where  $t$  is the potential flow lift /straight-line function tangent to the  $C_L$  curve at ( $\alpha = 0, C_L = C_L(0)$ ).

$$C_L = f \cdot t + (1 - f)s \quad (2.30)$$

Eqs. (2.30) gives a smooth interpolated transition from attached flow curve ( $t$ ) to fully separated flow ( $s$ ) since  $0 < f < 1$ . The transformation function can be formulated using Eqs. (2.31).

$$f = \frac{1}{(1 + k \cdot \Delta\alpha^4)} \quad (2.31)$$

where

$$k = \left(\frac{1}{f_2} - 1\right) \cdot \frac{1}{(\alpha_2 - \alpha_m)^4} \quad (2.32)$$

The angle of attack,  $\alpha_m$  is defined as in Eqs. (2.33), the angle where the  $C_L$  curve starts to deviate from the potential curve ( $t$ ).

$$\alpha_m = \frac{\alpha_1 - G\alpha_2}{1 - G} \quad (2.33)$$

where

$$G \equiv \sqrt[4]{\frac{\frac{1}{f_1} - 1}{\frac{1}{f_2} - 1}} \quad (2.34)$$

The drawback of this approach is that the assumptions on this method is not supported by a wide set of experimental data with different sections along the blade span to sufficiently support the assumptions of this methods.

#### 2.1.4 Turbine Model

This research project used a vertical-axis turbine with a single rotor blade only. This design was chosen because the primary goal of this research is to investigate the effects of airfoil aerodynamics due to the polar extrapolation approach on the turbine performance. Nevertheless, only a single rotor blade was utilized to reduce the complexity of the simulation. The blade profile used is the airfoil NACA 0018, as illustrated in Figure 2.7.

NACA 0018 is an airfoil that is commonly employed in wind energy applications. The benefits of using this NACA 0018 as blade profile have detail described in section 1.4. The subgoal of this project is also to create an annotated database of aerodynamic coefficients for this airfoil so that any researcher interested in using it in wind energy applications can get

accurate and reliable findings. Table 2.1 shows the detailed setup of each set of experimental data, numerical data, and present study data from QBlade.

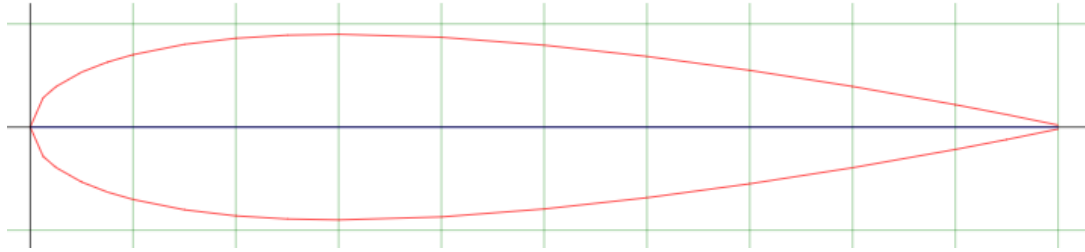


Figure 2.7: Airfoil NACA 0018.

Table 2.1: Summary of experimental and numerical airfoil polar data used for investigation.

ID	AOA range (°)	Reynolds number ( $10^3$ )	Turbulence intensity, I (%)	Surface roughness	Wind tunnel configuration	Blockage correction	Reference
Bianchini	0 - 180	300	Low (<0.1)	1000 grit sandpaper	Closed-jet $c/H=0.2$	ESDU76028	(Bianchini, Balduzzi, Rainbird, <i>et al.</i> , 2016)
Claessens	0 - 180	300	Low (<0.2)	aluminium	Closed-jet $c/H=0.20$	#N/D	(Claessens, 2006)
Longhuan Du	0 - 180	140	Low (<1)	RP unpolished	Closed-jet $c/H=0.28$	Garner & Roger	(Longhuan Du <i>et al.</i> , 2015)
Sheldahl & Klimas	0 - 180	360	#N/D	aluminium	Closed-jet $c/H=0.18$	Pope & Harper	(Sheldahl and Klimas, 1981)
Exp + Viterna	-180 - 180	150	-	-	-	-	(Bianchini, Balduzzi, Rainbird, <i>et al.</i> , 2016)
Exp + Montgomerie	-180 - 180	150	-	-	-	-	(Bianchini, Balduzzi, Rainbird, <i>et al.</i> , 2016)
CFD (URANS)	0 - 180	150	-	-	-	-	(Bianchini <i>et al.</i> , 2016; Melani <i>et al.</i> , 2019)
XFoil + Viterna	-180 - 180	300	-	-	-	-	Present study
XFoil + Montgomerie	-180 - 180	300	-	-	-	-	Present study

## 2.2 Simulation

From airfoil design and analysis to turbine design and simulation, this section delves into the QBlade software in depth. The line-lifting theory free vortex wake model and a low-

order computational model used to simulate turbine performance are also discussed in this section.

### 2.2.1 QBlade

QBlade is an open-source turbine calculation software proposed by the Wind Energy Group at the Berlin Technical University Department of Experimental Fluid Mechanics in 2010. The aim of the software is to provide a single-solution software for designing and calculating the aerodynamics of wind turbine blades without requiring data from other sources to be imported, converted, or processed (David Marten and Wendler, 2013a). The core functionality of QBlade consists of airfoil design and analysis module, polar extrapolation module, blade design and optimization module, and turbine definition and simulation module as illustrated in Figure 2.8.

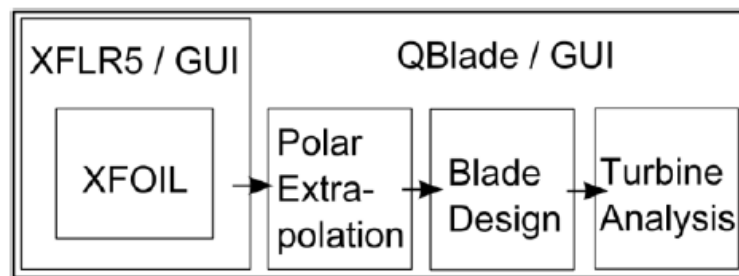


Figure 2.8: Basic software modules inside QBlade (D Marten and Wendler, 2013).

#### 2.2.1(a) Airfoil Design and Analysis

The simulation of turbine performance requires tabulated airfoil polar data, which are the lift and drag coefficients over a range of angles of attack. QBlade incorporates XFOIL which is a tool that utilize to construct and analyse subsonic isolated airfoils interactively. It allows users to design custom airfoils and calculate theirs polar rapidly. Airfoils can be designed via a NACA airfoil generator, splines, or imported from a point distribution, as shown in Figure 2.9. XFLR5 software is an analysis tool for low Reynolds number airfoils, wings and planes that contains the XFOIL's direct and inverse analytical capabilities. It has also be implemented